JMEPEG (2019) 28:926–937
https://doi.org/10.1007/s11665-019-3883-3

1059-9495/$19.00

Effect of Niobium on the Secondary Precipitates and Tempering Resistance of Spray-Formed M3:2 High-Speed Steel

Hebin Wang, Longgang Hou, Yabin Li, Ping Ou, Li Shen, Xinger Wen, Hua Cui, and Jishan Zhang

(Submitted May 23, 2018; in revised form November 21, 2018; published online January 22, 2019)

The precipitation of secondary carbides in spray-formed M3:2 high-speed steels with or without 2% niobium (Nb) addition during overtempering at 600 °C was characterized, and the carbides were identified in detail using transmission electron microscopy. Strengthening in the peak-hardened state is due to coherent precipitates of types MC and M_2C. During overtempering, the hardness of M3:2 steel greatly decreases due to M_2C coarsening with the precipitation of M_3C carbide, whereas the very fine and dense nature of the M_2C precipitates is responsible for the remarkable long-time strength exhibited by the Nb-containing steel. The MC precipitates, however, are fairly stable. The addition of Nb results in substantial dissolution of Mo and Cr into the matrix prior to tempering, which refines the secondary M_2C precipitate dispersion and delays overaging reactions; therefore, superior tempering resistance can be obtained.

Keywords M3:2 high-speed steel, niobium, secondary carbide, spray forming

1. Introduction

High-speed steels (HSSs) are typically used for multi-point cutting tools and cold working tools due to their properties of high hardness, wear resistance, high strength, and excellent toughness (Ref 1, 2). In the conventional ingot metallurgy process, a population of blocky carbides are typically in the form of a dendrite or conglomeration eutectic by crystallization from the melt; these carbide arrangements will result in severe segregation, which reduces the hot workability of HSSs and deteriorates their properties (Ref 3). Powder metallurgy (PM), which was developed to fabricate HSSs with refined microstructures and a homogenous distribution of carbides, offers improved properties over conventional cast wrought products. However, PM typically involves a complex process and high costs associated with hot isostatic pressing (HIP) and low production rates (Ref 4, 5). During the past decades, spray forming (SF) technology has been proved to be a cost-effective way to produce of HSSs with low-level macrosegregation and fine carbides due to the high cooling rate during melt atomization and unique advantages of a one-step forming process (Ref 6-12).

In recent years, relatively inexpensive alloying elements, for example, silicon, niobium or titanium, have been widely used as a substitute in the HSSs for particularly expensive and scarce alloying elements, such as cobalt, molybdenum (Mo), and vanadium (V) (Ref 13-16). Among such elements, Nb has a higher affinity with carbon that V and can form a stable and hard MC-type carbide. In past studies, researchers have focused on the influence of Nb on the primary carbides or friction performance of HSSs (Ref 17-21); however, our understanding of the evolution behavior of secondary carbides precipitated during tempering is inadequate. Wang and Dunlop (Ref 22) systematically studied the secondary carbides in several PM HSSs, all of which showed two types of precipitates: disk-shaped MC and rod-like M_2C. The chemical components of precipitates are complex, as all alloying elements exist in both types of precipitates. In addition, steel containing 3.2 wt.% Nb shows a trace amount of Nb (0.1 at.%) in the matrix after hardening, 2 at.% Nb in MC, and 1.2 at.% Nb in M_2C after tempering (Ref 23). Researchers have reported that when the tungsten (W) or Mo in wrought M2 steel is replaced by large amounts of Nb, the hardness decreases (Ref 24). These results imply that the influence of Nb on the secondary precipitates in HSSs during tempering is insignificant. However, researchers have also reported a superior secondary hardness in Nb alloying steels after exceeding the maximum hardness, e.g., Dobrzański et al. (Ref 13) observed that fine M_4C_3 carbide precipitates distributed in the tempered matrix resulted in a higher secondary hardness than that of the HSSs without Nb addition. Similar results were obtained by Karagöz and Fischmeister (Ref 17), who found that the secondary hardness of the Nb-alloyed PM steel (2% W, 3% Mo, 1.6% V, 3.2% Nb) persisted at higher temperatures than that of AISI M2. It was also reported that the high temperature hardness could be maximized by replacement of 0.8 wt.% of W with an equivalent Nb content (Ref 15). Previous studies have shown that the addition of 0.5-2 wt.% Nb to spray-formed M3:2 HSSs can refine the carbide and improve the mechanical properties (Ref 19, 25). In addition, a superior tempering resistance of 2% Nb-alloyed steel is acquired by high-density M_2C nanoparticles (Ref 26). However, the precipitate evolution in HSSs as a function of overaging time is

Hebin Wang, Yabin Li, Ping Ou, Li Shen, and **Xinger Wen**, School of Materials Science and Engineering, Jiangxi University of Science and Technology, Ganzhou 341000, China; **Longgang Hou, Hua Cui,** and **Jishan Zhang**, State Key Laboratory for Advanced Metals and Materials, University of Science and Technology Beijing, Beijing 100083, China. Contact e-mails: wanghemse@163.com, lghou@skl.ustb.edu, and cnopyp@163.com.

still poorly understood. In addition, the relation between the matrix composition and precipitate characterization and its relation to the change in hardness require further study.

In this work, M3:2 high-speed steel billets with a adjusted composition with the partial substitution of V in this steel by about 2 wt.% Nb for improving the anti-abrasive properties and high temperature stability were prepared by spray forming. The aim of this work was to characterize the precipitation of secondary carbides in a spray-formed M3:2 HSSs during overtempering. In the present study, the hardness of steels after tempering at 500-650 °C was investigated. The morphology and distribution of carbide and the phase composition of HSSs after overtempering at 600 °C were characterized. The influence of Nb on the secondary precipitates and tempering resistance of HSSs is also discussed.

2. Experimental Procedure

The chemical compositions of the two experimental steels were Fe-1.29C-6.37 W-5.11Mo-4.12Cr-2.97V (M3:2, wt.%) and Fe-1.31C-6.29 W-5.03Mo-4.16Cr-2.05V-1.95Nb (MN2, wt.%). Both steels were prepared by SF using the facility in University of Science and Technology Beijing (USTB). The molten alloys with a superheat of 150 K were atomized by a free fall atomizer and spray-deposited on a rotating substrate, resulting in cylindrical billets. The atomization gas pressure and the deposition distance were 0.5 MPa and 450 mm, respectively.

To eliminate porosity in the deposits, cylindrical bars (60 mm diameter and 80 mm length) cut from deposited billets were hot-forged to 16 mm diameter at a temperature of 950-1150 °C. After isothermal annealing at 860 °C for 4 h followed by slow cooling to 750 °C and holding at 750 °C for 6 h, the samples were slowly cooled to 500 °C and then cooled down in air. The specimens were exposed to a heat treatment that is typical for the tool steels they represent: austenitizing at 1180 °C for 10 min, followed by quenching and triple tempering for 1 h at 500-650 °C. After the standard triple tempering treatment at 560 °C, the alloys were isothermally overtempered at 600 °C for 24-168 h. Thin foils for transmission electron microscopy (TEM, H-800, and FEI Tecnai F20 microscopes operated at 200 kV) were prepared by twin-jet electropolishing 3-mm-diameter disks at − 10 °C in a solution of 10% perchloric acid, 15% glycerol, and 75% ethanol at a current of approximately 30 mA. Energy-dispersive x-ray spectroscopy (EDX) was employed for local chemical composition analysis. Analyses were made for more than 15 different particles or positions within each phase so that a satisfactorily low standard deviation could be obtained from the measurements. The sizes and number density of different precipitates were determined using the quantitative image analysis software (Image-Pro Plus 6). Ten fields of each sample were taken at a magnification of 80,000 × for temper times up to 3 h and at 120,000 × for longer times. The total number of particles measured ranged from approximately 600-3000, depending on tempering temperature and time. Hardness measurements were performed on the materials after various tempering processing using specimens with dimensions of 10 mm × 10 mm × 10 mm, and ten readings were used to obtain an average value to reduce the error for each sample.

3. Results

3.1 Effect of Nb on the Hardness of HSSs

The Vickers hardness was measured as a surrogate for strength for the two experimental steels after triple tempering treatments of 3 × 1 h as a function of the tempering temperature. With respect to the hardness (Fig. 1a), the secondary hardening phenomenon appears, beginning at 500 °C and reaching a maximum at 560 °C. When the tempering temperature exceeds 560 °C, the hardness decreases gradually. However, the secondary hardness of MN2 persists to somewhat higher temperatures. With respect to tempering at 650 °C, an increase in approximately 50 points on the Vickers scale, equivalent to an increase in approximately two points on the Rockwell C scale, compares quite favorably with the early data of Karagöz (Ref 17), which show secondary hardening in martensite to be approximately 2 HRC for 3.2% Nb-alloyed steel. The effect of overtempering at 600 °C on the hardness of the triple tempered steels is shown in Fig. 1(b). The hardness of the steels decreases with increasing overaging time, as MN2 steel possesses higher hardness than M3:2 steel. For the time period from 3 to 24 h, there is a difference of approximately 30 HV between these two alloys. For a longer duration, this advantage of the Nb-containing alloys is further improved: At 96 h and above, MN2 steel maintains a hardness of 70-90 HV higher than M3:2. The changes of hardness suggest the process of precipitation and growth of carbides and the recovery and recrystallization of the matrix.

3.2 Microstructure of As-Quenched Steels

After the hardening treatment but prior to tempering, the microstructure of both steels consists mainly of coarse globular primary MC and M_6C carbides embedded in the matrix, as shown in Fig. 2(a) and (b). Most of these carbides (3-6 μm) are dislocated in the grain boundaries, and some refined undissolved carbides with sizes of 0.2-1 μm are distributed inside the grains. During TEM observation, heavily twinned plate martensite is detected, as shown in Fig. 2(c) (the illustration shows the (012) matrix plane with the $(1\bar{2}1)$ twin axis identified by an arrow). Many fine twins may result from the high content of carbon and alloying elements. The high contrast of the martensite grain boundaries seems to be due to a high density of dislocations very close to the boundary. Additionally, some refined carbide particles with sizes of approximately 0.3-0.5 μm are observed to be dispersed in heavily twinned plate martensite (Fig. 2c and d). Electron diffraction showed that these carbides were either MC or M_6C types, which is consistent with the observation in Fig. 2(a) and (b).

3.3 Precipitation During Triple Tempering Treatment at 600 °C

As a result of repeated tempering above 500 °C and cooling to room temperature, the hardness of investigated steels increases gradually. In both alloys, the standard triple tempering treatment at 560 °C resulted in the transformation of retained austenite to martensite and fine-scale precipitation of secondary carbides, which are typically composed of V-rich MC and Mo-rich M_2C types (Ref 27-31). Typical examples of the TEM observations are given in Fig. 3. The tempered M3:2 steel consists predominantly of plate martensite, and very fine and

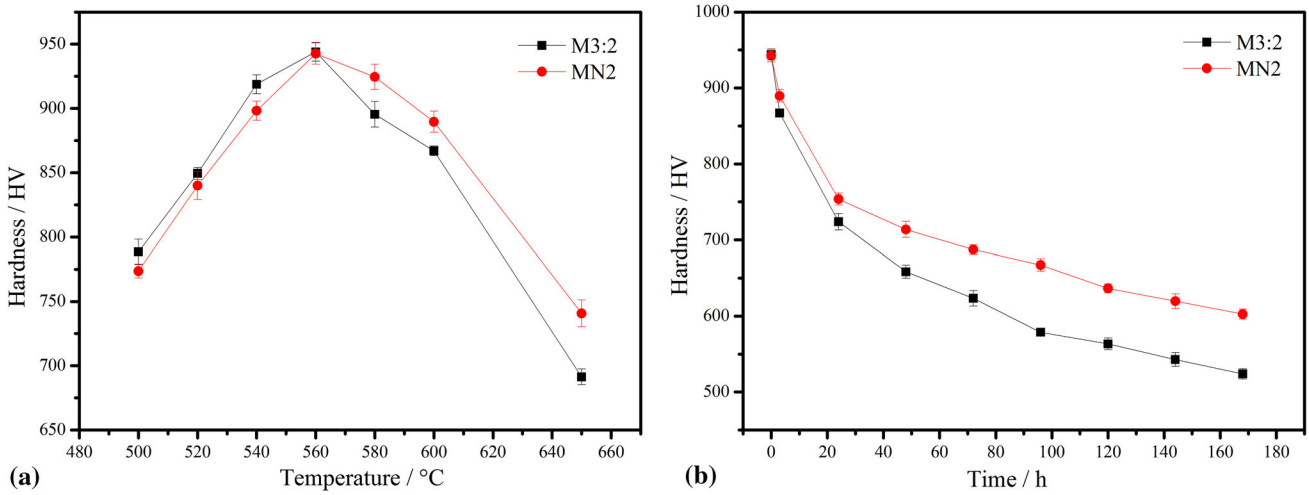

Fig. 1 Hardness of M3:2 and MN2 as a function of tempering temperature after triple 3 × 1 h heat treatment (a); effect of overtempering at 600 °C on the hardness of M3:2 and MN2 (b)

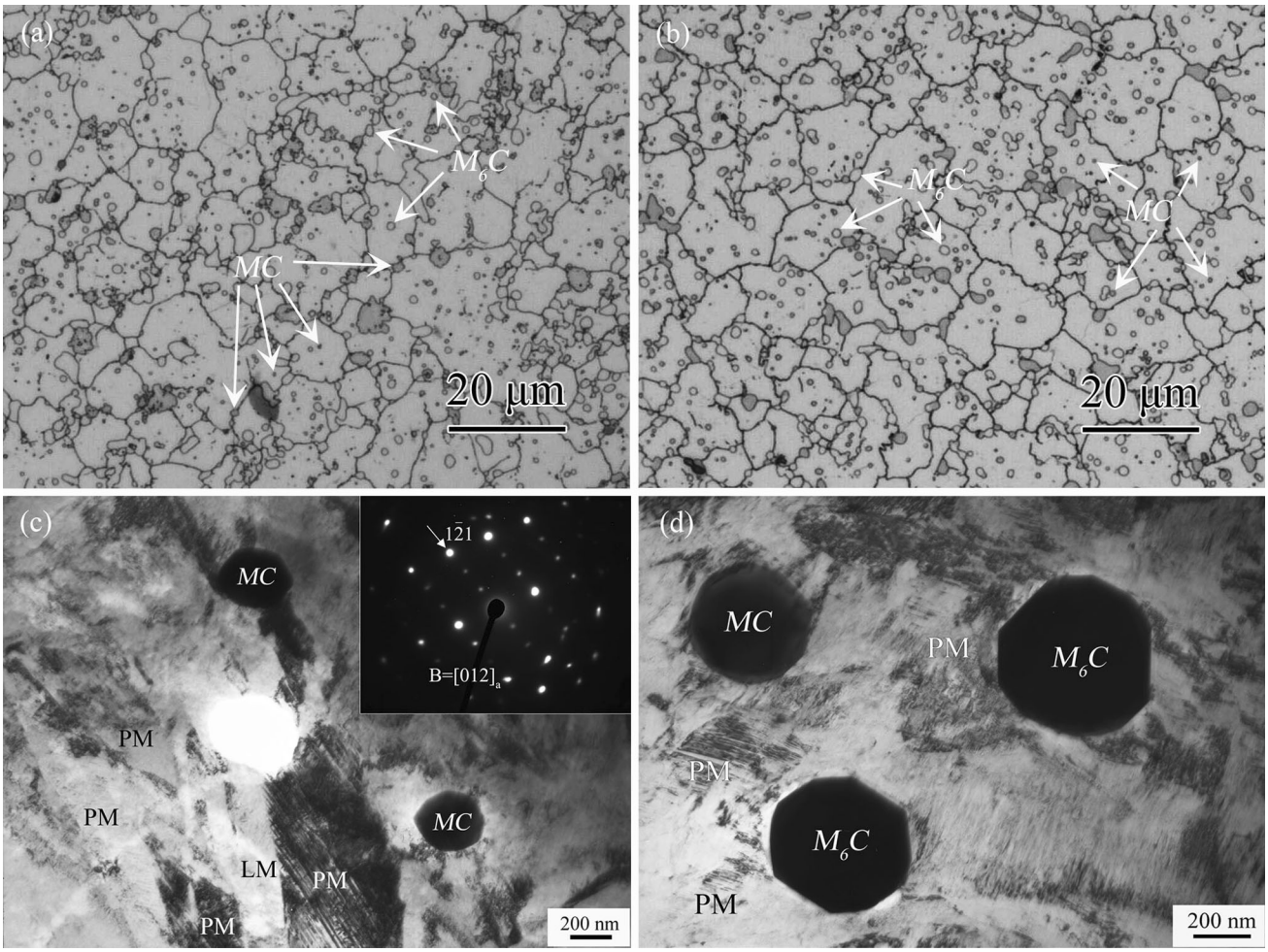

Fig. 2 Optical micrograph of the as-quenched MN2 (a) and M3:2 (b); TEM morphology of the martensite and primary carbides in the as-quenched MN2 (c) and M3:2 (d), PM and LM represent plate martensite and lath martensite, respectively

dense secondary carbides are precipitated both on the martensite plate boundaries and within the plates. The MC precipitates are plate-like and precipitated on the $\{001\}_\alpha$ habit planes, while the M_2C precipitates are needle shaped with the needle axis parallel to the $[001]_\alpha$ directions. M_2C has an hcp crystal structure and is generally considered to precipitate according to

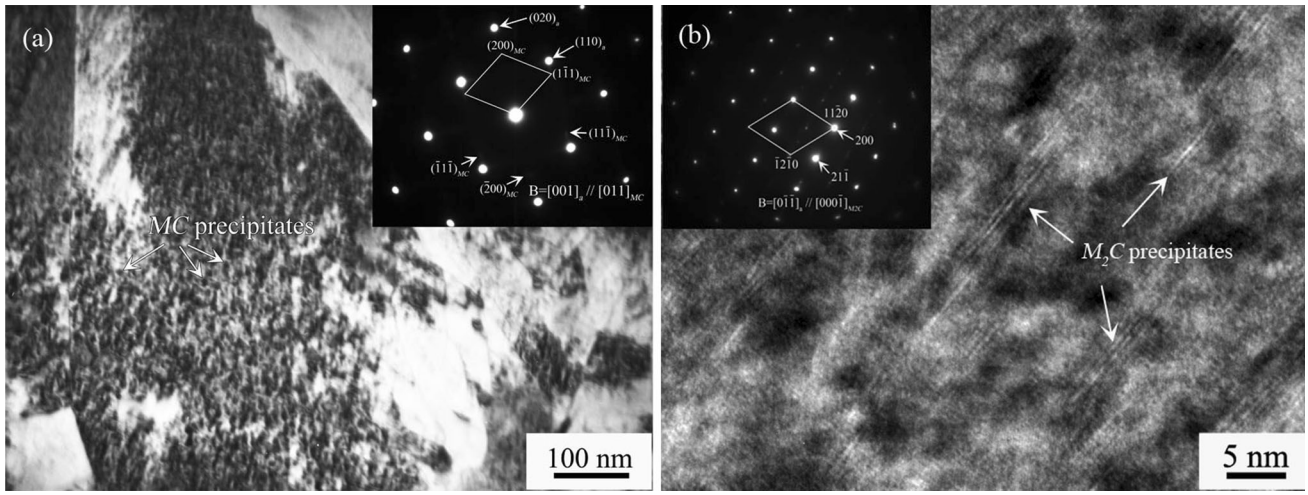

Fig. 3 Secondary precipitation of MC (a) and M_2C (b) in plate martensite after triple tempered at 560 °C in M3:2

the Pitsch–Schrader orientation relationship, i.e., $(0001)_{M2C}//(011)_\alpha$; $(\bar{1}100)_{M2C}//(011)_\alpha$; $(11\bar{2}0)_{M2C}//(100)_\alpha$. Another orientation relationship between M_2C and ferrites at short tempering times was found by Wang (Ref 32), i.e., $(0001)_{M2C}//(021)_\alpha$; $(11\bar{2}0)_{M2C}//(100)_\alpha$; $(\bar{1}100)_{M2C}//(01\bar{2})_\alpha$. For both orientation relationships, the M_2C precipitates are rod-like in shape, and the growth direction is $< 11\bar{2}0 >_{M2C}// < 100 >_\alpha$. As shown by the selected area diffraction pattern in Fig. 3(b), the M_2C precipitates were related to the ferrite lattice by the Pitsch–Schrader orientation relationship. The approximate size of MC platelets and M_2C rods in both steels was approximately 3-5 nm, 10-15 nm in length, and 1-2 nm in thickness. No substantial difference in the precipitate size was noted at the standard tempering between these two alloys.

TEM images (Fig. 4) of the overtempered specimens clearly show the MC and M_2C precipitates. As shown in Fig. 4(a), the precipitation of needle-like M_2C carbides evenly distributed in the microstructure of M3:2 became more prevalent after 3 × 1 h at 600 °C. It was also observed that the needle-like M_2C carbides were widely distributed along a particular direction in the plate martensite, which indicates that the rod axis or growth direction of M_2C is arranged in one set of possible planes, as mentioned before. The size of M_2C precipitates in this state is measured to be approximately 15-40 nm in length. Figure 4(b) shows the needle-like M_2C precipitates in the matrix of MN2 steel with identical conditions; in contrast, most of the needles are 15-20 nm in length. Relative to the observations in the peak-hardened state, the original M_2C secondary carbides in M3:2 have coarsened (from 10-15 to 15-40 nm) after 3 × 1 h at 600 °C, and this effect occurred to a lesser degree (from 10-15 to 15-20 nm) in MN2 steel.

Figure 4(c) and (d) shows the morphologies of the very fine MC secondary carbides in M3:2 steel tempered at 600 °C for 3 × 1 h. Numerous fine platelets, approximately 5-8 nm in length and 1-2 nm in thickness, are distributed in the martensite matrix. The corresponding selected area diffraction pattern from these areas indicates that these plate-like precipitates are MC carbides and that the lattice of the MC precipitates was oriented with respect to the ferrite matrix according to the Baker–Nutting orientation relationship, i.e., $(100)_{MC}//(100)_\alpha$. As shown in Fig. 4(c), the $\{200\}_{MC}$ reflections were generally streaked in the $< 200 >_\alpha$ directions, indicating that the habit plane of the MC platelets is $\{100\}_\alpha$. This finding was confirmed by the dark-field electron micrograph of MC carbides using $(200)_{MC}$ reflection; as shown in Fig. 4(d), the plate-shaped MC precipitates are found to be distributed along the $\{200\}_\alpha$ planes. No significant difference exists in the distribution and magnitude of MC carbides between these two alloys. Consequently, it is clear that the characterization of morphology and distribution of the MC carbides exhibited no prominent changes during triple tempering at 560-600 °C, suggesting that the fine MC-precipitated carbides in the alloys are thermodynamically stable and show little tendency to coarsen even after triple tempering at 600 °C.

3.4 Overaging at 600 °C

Specimens of M3:2 and MN2 steels that had been previously given the standard triple tempering treatment at 560 °C were further aged for 24-168 h at 600 °C as an overheating treatment, which can occur during operation and degrade the material properties.

Figure 5 shows the changes in the precipitate distribution of M3:2 steel after 96 h at 600 °C. As shown in Fig. 5(a), the coarsened M_2C needles that were 30-40 nm in length are found to be distributed in the plates, and their rod axes are mutually perpendicular. The size of the MC precipitate plates was estimated to be approximately 5-8 nm in length and 1-2 nm in thickness (Fig. 5b). In addition, the precipitation of other ellipsoidal carbides measuring 20-80 nm in length both on the interfaces and within the matrix can be observed (Fig. 5a and c). The corresponding selection diffraction patterns of the carbides show unambiguously that they are of orthorhombic M_3C type, containing a large proportion of Fe and a small portion of Cr, Mo and W (Fig. 5e). The diffraction pattern results in conjunction with the insert of Fig. 5(c) indicate that the long axes of M_3C carbides were parallel to the $< 110 >_\alpha$, consistent with the orientation relationship of M_3C with α-iron as reported by Wells (Ref 33).

The morphology and distribution of the precipitates in MN2 steel tempered at 600 °C for 96 h are shown in Fig. 6. Numerous fine needle-like carbides measuring 10-20 nm in length and plate-shaped particles (approximately 5 nm in diameter) were found to coexist in the martensite matrix (Fig. 6a), with the selected area diffraction results, suggesting that the secondary precipitates were either M_2C satisfying the

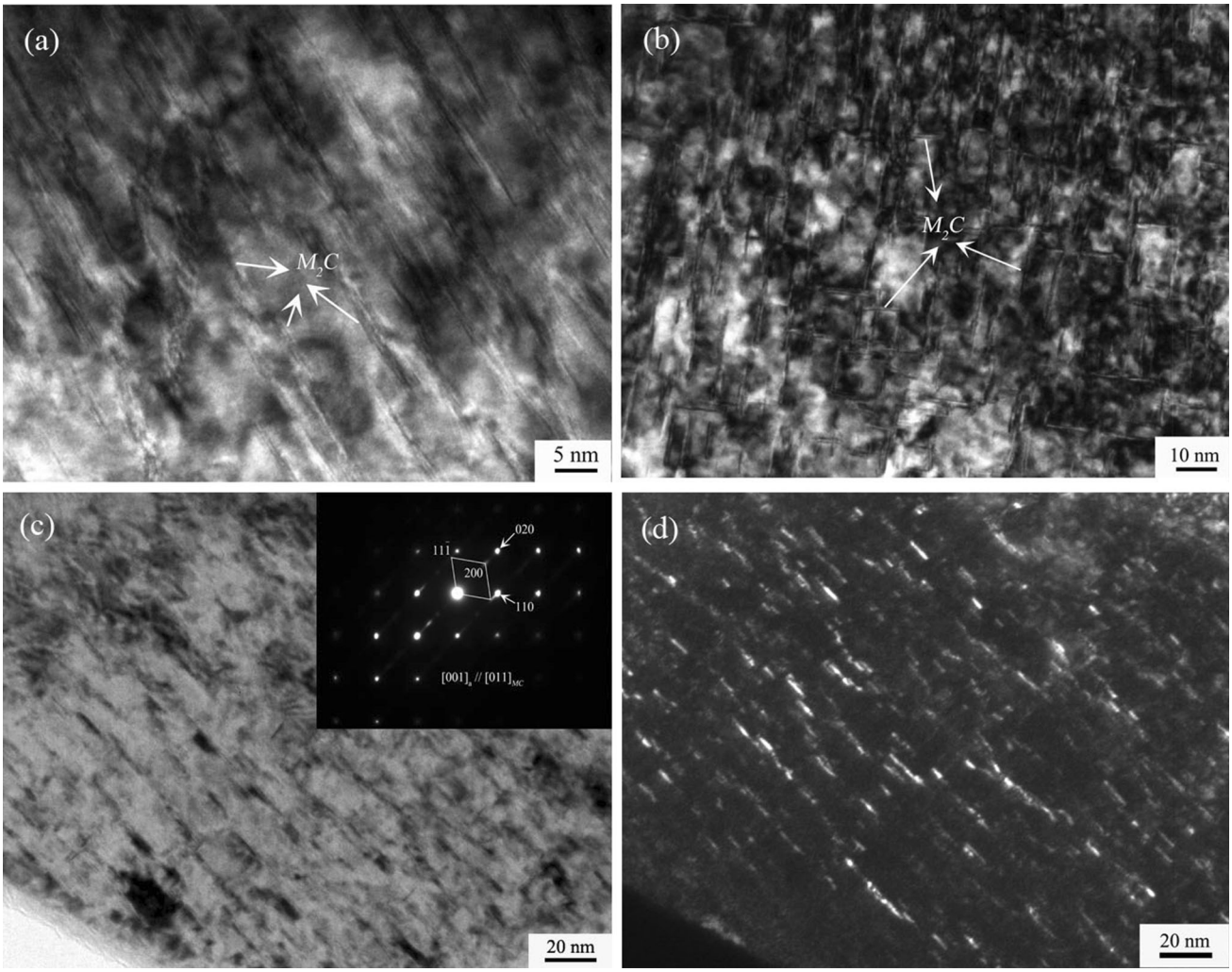

Fig. 4 Secondary precipitation of M_2C in plate martensite of M3:2 (a) and MN2 (b) during tempering 3 × 1 h at 600 °C; bright field (c) and dark field (d) of secondary carbide MC in M3:2

Pitsch–Schrader crystallographic orientation relationship with the matrix or MC satisfying the Baker–Nutting orientation relationship. Furthermore, the growth direction of M_2C needles was found to be parallel to $<100>_\alpha$, as mentioned previously. In addition, ellipsoidal M_3C carbides (approximately 50 nm) are occasionally detected within the martensite of MN2 steel (Fig. 6b); these particles are rich in Fe but include a significant portion of Cr and a certain amount of Mo and W (Fig. 6c). The M_3C precipitates tend to be larger and more populated in M3:2 than in the MN2 steel, and it was apparent that the depletion of M_2C and MC in the vicinity of M_3C precipitates occurred during overaging, which indicates that the coarse M_3C grew at the expense of the fine M_2C and MC secondary carbides.

When the overaging time was elevated to 168 h, considerable changes occur in the microstructure of steels. A typical bright field micrograph of M3:2 steel is shown in Fig. 7(a) and (b); the microstructure change in the plate morphology of martensite is prominent, and the dislocation density has decreased significantly. Note that the original dispersion of M_2C precipitate has disappeared at this stage; as a replacement, an aggregate of M_3C appeared as long rod-like shapes (120-400 nm) mostly distributed on the boundaries of the internal twins and also within the matrix. Figure 7(e) presents the average element concentrations in M_3C (Ref 26); note that the chemical composition of M_3C carbides is not greatly changed. As shown in Fig. 7(a), the rod-like M_3C is found to be distributed in the matrix with a separation of 70 degrees (Ref 26). Wells et al. (Ref 33) showed that the orientation relation of M_3C with α-iron is $(001)_{M3C}//(112)_\alpha$ and that the long axes of M_3C needles are parallel to the $[010]_{M3C}$ and the $[111]_\alpha$ direction. It is generally known that the angle between $<111>_\alpha$ is 70.53 degrees, consistent with the results observed in Fig. 7(a). Relative to the M_3C carbide precipitation in M3:2 after tempering for 96 h at 600 °C, the original fine M_3C carbides have coarsened substantially, and strong coarsening has reduced the density of M_3C precipitates in the plates. In the case of MN2 steel, notably, very fine M_2C secondary precipitates with a high number density are still observed even after such prolonged aging treatment (Fig. 7c), and a great number of needle-like M_2C precipitates (20-50 nm in length and 3-4 nm in thickness) are found to be evenly distributed in the matrix. The corresponding selected area diffraction pattern from this area indicates that the M_2C precipitates are also related to the ferrite lattice by the Pitsch–Schrader orientation relationship. On the other hand, a few shorter M_3C carbides containing a large proportion of Cr, Mo and W (Fig. 7f) are

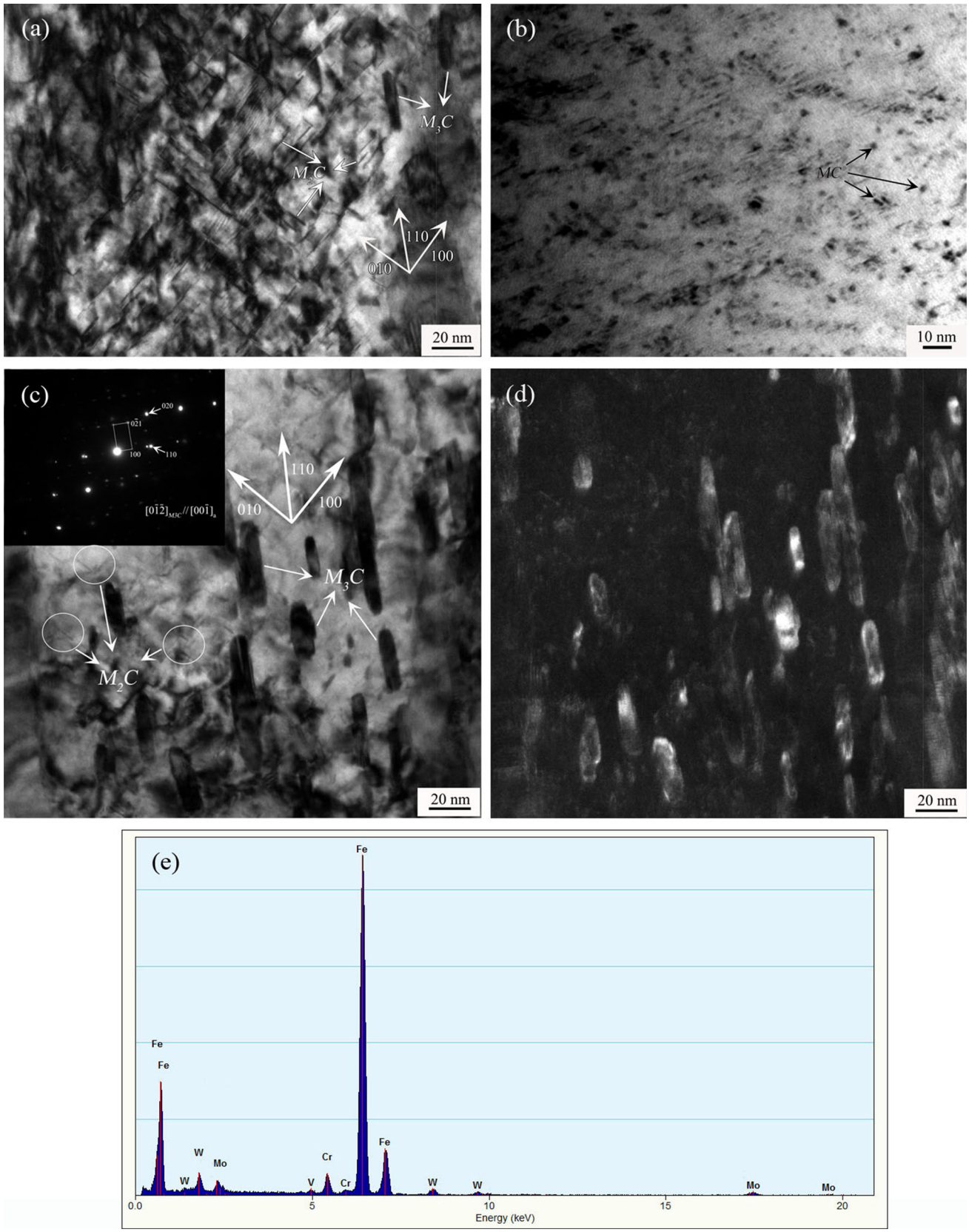

Fig. 5 Coarsened M_2C needles and ellipsoidal M_3C carbides (a) and precipitation of MC (b) in M3:2 after overaging 96 h at 600 °C; depletion of fine secondary carbide dispersion of M_2C and MC around the M_3C precipitates: (c) bright field; (d) dark-field image using $(001)_{M3C}$ reflection; typical energy-dispersive spectra of M_3C carbides in M3:2 (e)

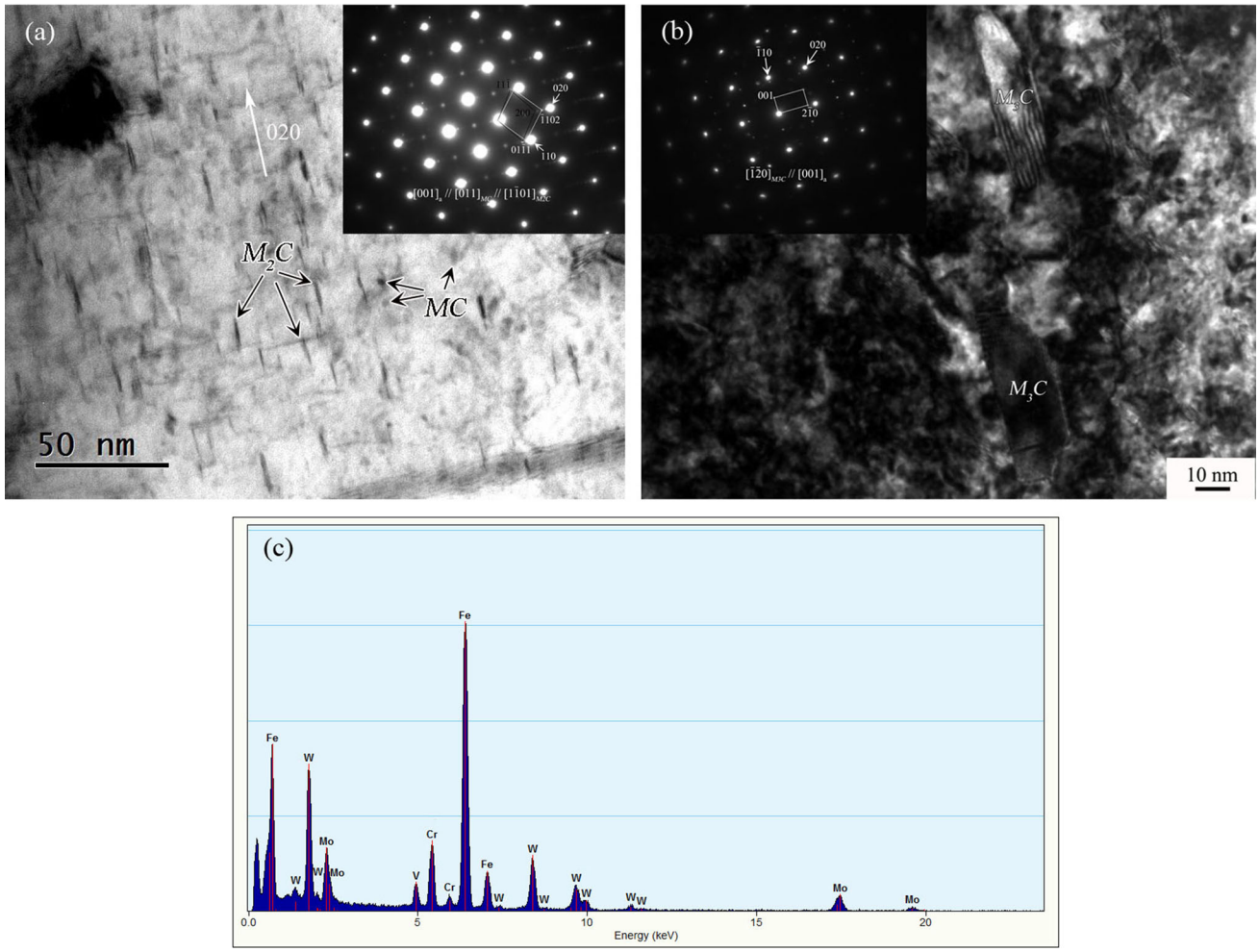

Fig. 6 Secondary precipitation of M_2C (a) and orthorhombic M_3C carbide (b) in MN2 after overaging 96 h at 600 °C; typical energy-dispersive spectra of M_3C carbide in MN2 (c)

found to coexist with the fine M_2C precipitates, which indicates that the Cr and Mo atoms continue to enter the M_3C particles during this period. In addition, the fine precipitate dispersion of MC plates is readily observed in the matrix (Fig. 7d); the size of MC plates is approximately 5-10 nm in length and 2-3 nm in thickness, and there is no substantial difference in MC precipitate size between these two alloys.

TEM observation shows that martensite in both steels was partially recrystallized and transformed into polygonal ferrite. After tempering for 168 h at 600 °C, the plate martensite structure in MN2 had recovered, and the microstructure consisted of polygonal ferrite with relatively coarse particles of $M_{23}C_6$ and M_6C (Fig. 8b, c, and d). These precipitates often nucleated at the interfaces of primary carbides with the ferrite matrix and martensite plate boundaries, in which they acted as pinning points for the subgrain boundary network. It was also found that the martensite did not completely decompose when tempered for 168 h and that the dislocation density in some areas remains very high, and equiaxed ferrite subgrains with M_6C precipitates at subgrain boundaries were presented (Fig. 8a). Compared to the composition of matrix in the state of as quenched, or even to the matrix composition after triple tempering at 560 °C, the content of Cr, Mo, and V in the matrix had been consumed substantially by the precipitates.

4. Discussion

The quantified particle sizes and number densities during tempering are collected in Table 1. In agreement with the qualitative observations, the size of MC precipitates was relatively constant at all stages, and the number density of the MC precipitates in both steels seems to increase at early stages of overtempering and then reached a maximum at 600 °C for 96 h. By contrast, the density of M_2C particles exhibited a constant decrease during overaging, and the very fine M_2C precipitates tended to coarsen and ultimately dissolve to be replaced by the M_3C carbide phases. In MN2 steel, the coarsening process seems to progress in a similar fashion at all stages; however, the M_2C particles precipitate in higher densities and coarsen less rapidly than those in M3:2 steel. Combined with the microstructure observation, the evidence indicates that the addition of Nb has a very strong effect on the nature and distribution of the precipitates after overtempering. In general, two important differences were detected with respect to M3:2 and MN2 steels: Much denser needle-like M_2C particles within the plates are found in MN2 steel, but a larger and coarser distribution is found in the M3:2 steel. On the other hand, ellipsoidal M_3C carbides were eventually generated

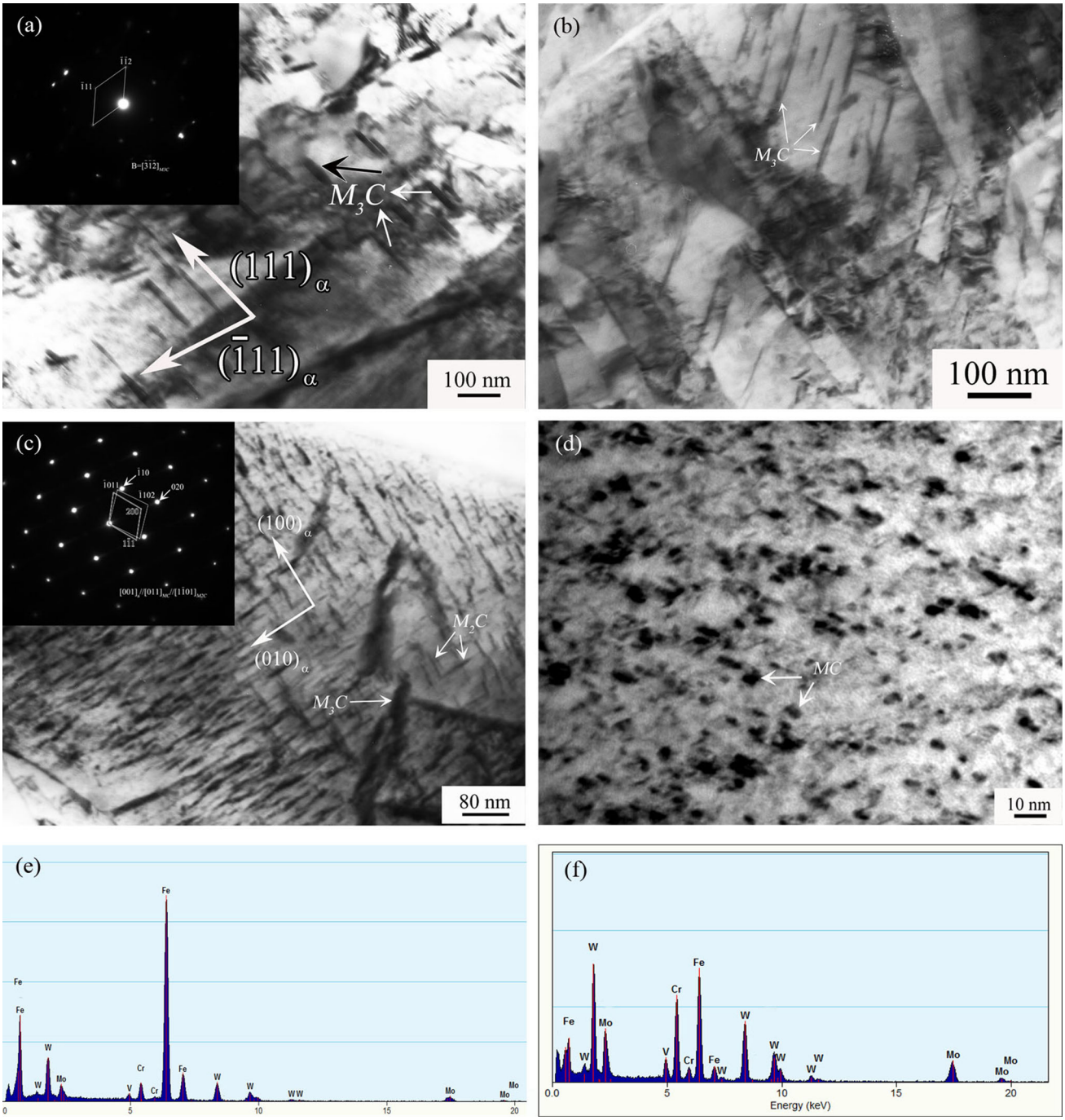

Fig. 7 M_3C carbide precipitation (a, b) in M3:2 after overaging for 168 h at 600 °C; M_2C secondary precipitates with small amounts of M_3C carbide in MN2 (c); MC secondary precipitates in MN2 (d); typical energy-dispersive spectra of M_3C carbide in M3:2 (e) and MN2 (f)

within the martensitic plates in M3:2 steel, developed at the expense of the fine MC and M_2C precipitate dispersion, but the formation and growth of M_3C can be inhibited in MN2 steel.

To understand the effect of Nb addition on the secondary carbide formation, it is important to relate the tempered microstructure to the earlier composition and amount of globular primary carbides observed after quenching. As shown in Table 2, the primary carbides had complex mixed compositions. As may be expected, V was strongly concentrated in the MC primary carbides while W and Mo were the alloying elements primarily responsible for the formation of M_6C. Previous studies have shown that the M_2C eutectic carbides can be transformed into M_6C eutectic carbides by 2% Nb addition (Ref 34) and that the M_6C carbides in MN2 steel contained a lower content of Mo than those in M3:2 alloy; in addition, the fraction of Mo and Cr in the primary MC-type carbides are also lower in steels with Nb addition (as shown in Table 2). Thus, a large number of Mo and Cr atoms were dissolved into the martensitic matrix prior to tempering.

In the case of tempering, the composition of matrix changes with increasing alloy carbide. As shown in Table 2, almost all the carbide-forming elements participate in the formation of

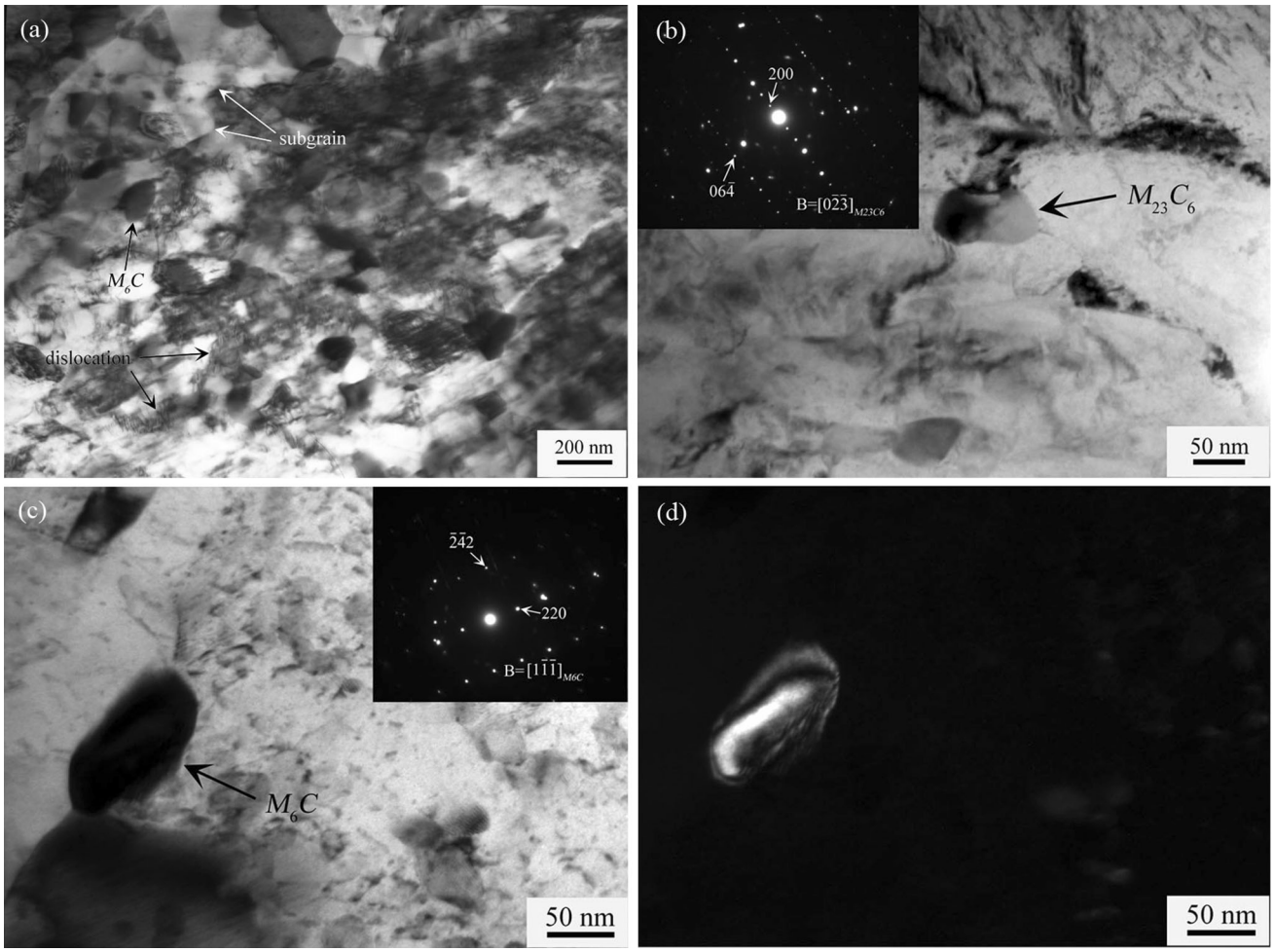

Fig. 8 Partially recovered grains with dislocation network in MN2 after overaging for 168 h at 600 °C (a); TEM morphology of $M_{23}C_6$ (b) and M_6C (c, d) carbide, (c) bright field, (d) dark-field image using $(220)_{M6C}$ reflection

Table 1 Typical size, density and distribution of the secondary precipitates in the tempered steels

Steel	Treatment	Precipitate type	Density, 10^9/mm^2	Size, nm	Distribution
M3:2	560 °C/3 × 1 h	MC	13.1	3-5 × 2	Inside plates and along boundaries
		M_2C	31.6	10-15 × 2	Inside plates
	600 °C/3 × 1 h	MC	18.2	5-8 × 2	Inside plates and along boundaries
		M_2C	20	15-40 × 3	Inside plates
	600 °C/96 h	MC	29.8	5-8 × 2	Inside plates and along boundaries
		M_2C	10.5	30-40 × 3	Inside plates
		M_3C	0.7	50-80 × 18	Inside plates and along boundaries
	600 °C/168 h	MC	15.75	5-10 × 2	Inside plates and along boundaries
		M_3C	0.4	120-400 × 20	Inside plates and along boundaries
MN2	560 °C/3 × 1 h	MC	11.6	3-5 × 2	Inside plates and along boundaries
		M_2C	36.3	8-12 × 2	Inside plates
	600 °C/3 × 1 h	MC	15	5-8 × 2	Inside plates and along boundaries
		M_2C	29.7	10-20 × 2	Inside plates
	600 °C/96 h	MC	27	5-8 × 2	Inside plates and along boundaries
		M_2C	20.1	15-20 × 2	Inside plates
		M_3C	Few	50 × 15	Inside plates and along boundaries
	600 °C/168 h	MC	13.9	5-10 × 2	Inside plates and along boundaries
		M_2C	12.1	20-50 × 3	Inside plates
		M_3C	0.1	60-100 × 15	Inside plates and along boundaries

precipitates except for Nb because its concentration in the matrix remains low. In particular, a marked depletion of Cr, Mo and V is noted during the entire stage, which indicates that the Mo, Cr and V are primarily responsible for the precipitation of secondary carbides, while W does not participate very strongly in the formation of precipitates. Wang (Ref 22) showed that the

Table 2 Average STEM/EDX analyses of substitutional elements (at.%) in primary carbides and the martensite matrix before and after tempering. The indicated error limits are standard deviations of the spread between individual measurements

Steel	Carbide	W	Mo	Cr	V	Nb	Fe
M3:2	MC	9.1 ± 1.5	11.4 ± 1.5	4.0 ± 0.6	70.0 ± 5.2	…	Bal.
	M_6C	18.4 ± 1.4	22.4 ± 1.0	5.2 ± 0.6	6.8 ± 1.0	…	Bal.
	Matrix	0.9 ± 0.1	2.1 ± 0.1	4.1 ± 0.4	1.2 ± 0.1	…	Bal.
	560 °C/3 × 1 h	0.3 ± 0.2	1.4 ± 0.3	2.7 ± 0.2	0.6 ± 0.2	…	Bal.
	600 °C/3 × 1 h	0.3 ± 0.1	1.3 ± 0.4	2.3 ± 0.3	0.5 ± 0.1		Bal.
	600 °C/96 h	0.2 ± 0.1	0.6 ± 0.2	1.2 ± 0.3	0.5 ± 0.2		Bal.
	600 °C/168 h	…	0.4 ± 0.2	0.7 ± 0.1	0.3 ± 0.2		Bal.
MN2	MC	7.9 ± 1.8	7.1 ± 1.3	2.2 ± 0.6	21.0 ± 4.6	52.1 ± 5.8	Bal.
	M_6C	25.4 ± 1.4	13.8 ± 1.1	5.4 ± 0.4	4.2 ± 0.5	3.5 ± 0.5	Bal.
	Matrix	0.2 ± 0.1	3.1 ± 0.2	4.9 ± 0.3	1.1 ± 0.1	0.1 ± 0.03	Bal.
	560 °C/3 × 1 h	…	2.3 ± 0.4	4.1 ± 0.4	0.6 ± 0.1	…	Bal.
	600 °C/3 × 1 h	0.5 ± 0.2	1.8 ± 0.3	2.9 ± 0.1	0.7 ± 0.2	…	Bal.
	600 °C/96 h	0.3 ± 0.1	1.5 ± 0.3	2.4 ± 0.4	0.5 ± 0.1	…	Bal.
	600 °C/168 h	…	1.2 ± 0.2	2.1 ± 0.3	0.2 ± 0.1	…	Bal.

main carbide-forming elements in M_2C phase are Mo and Cr, while the MC phase contains mainly Cr, Mo and V. Similar results were also obtained by Fischmeister (Ref 23). It has been reported that the fineness of precipitates is associated with their mixed chemical constituents and that the incorporation of Cr in precipitates can favorably reduce the lattice parameters of both MC and M_2C, resulting in a reduction in the nucleation threshold and enhancement of the hardening effect (Ref 22, 32, 35, 36). Therefore, early precipitation may stabilize the heterogeneous nucleation size from recovery or recrystallization during tempering. Davenport observed a similar phenomenon in the secondary hardening response of W and Mo steels; in their study, they found that the Mo_2C dispersion was finer than the W_2C dispersion during tempering, and they attributed this imbalance to the much slower diffusion of W in ferrite relative to that of Mo (Ref 37). On the other hand, an alloy element diffuses into precipitates in proportion to its supply in the matrix prior to tempering. As shown in Table 2, the concentration of W in matrix is relatively low, while the content of Cr and Mo is high, particularly in MN2 steel, because the constitutive Cr and Mo in primary MC and M_6C decrease with Nb addition, so much more Cr and Mo can be dissolved into the matrix. Thus, a higher content of Mo and Cr in the matrix prior to tempering has a strong influence on the formation of finer and denser M_2C precipitates during tempering. In addition, the coarsening behavior of precipitates during overaging should be considered. According to the model of Bjorklund et al., the rate constant of the coarsening kinetics of M_2C is inversely proportional to K_M^2 (where K_M is the coarsening rate constant with alloying element M added), which suggests that the coarsening resistance of M_2C scales up with an increasing amount of dissolved solutes or alloying elements (Ref 38). A further study conducted by Lee et al. showed that the concentration of Cr and Mo in the matrix is the most important factor that determines the magnitude of K_M (Ref 39). This result is similar to that reported by Dunlop et al. (Ref 40). From this point of view, a much higher concentration of Mo and Cr in the matrix of MN2 steel not only refines the distribution of M_2C precipitates but also enhances the coarsening resistance of M_2C precipitates during overtempering.

Notably, coarsened M_3C measuring ~ 400 nm in length was observed in M3:2 steel after tempering 168 h at 600 °C; in contrast, only a few fine elongated M_3C carbide particles with a size of 60-100 nm were found within the plates and along the boundaries in MN2 steel (Fig. 7c). Considering the microstructure observation during tempering over 96 h at 600 °C, it seems likely that the coarsening rate of M_3C precipitates decreased with Nb addition. It is well known that M_3C in high alloy steels is $(Fe,M)_3C$, whose stability can be greatly affected by the addition of alloying elements. With respect to M3:2 steel, due to the lower content of Cr in M_3C, the growth of the M_3C carbide during overtempering is expected to be controlled by carbon diffusion and is thus very rapid. In that case, with the substantial precipitation of ellipsoidal M_3C carbides, the concentration of carbon in the matrix decreases, leading to a reduction in the solution strengthening effect. On the other hand, the dispersion strengthening effect of relatively coarse M_3C particles is lower than that of fine MC and M_2C precipitates; therefore, the hardness of the tempered M3:2 steel decreases. For the MN2 steel, during overtempering, a substantial amount of Cr acquires sufficient mobility (enabling the formation of precipitates) and diffuses to the M_3C particles, which improves the stability and constrains their growth during overtempering. Considering the microanalysis traces of M_3C particles in M3:2 and MN2 steels after the 168 h treatments at 600 °C, it is notable that more Cr atoms enter the M_3C particles, as shown in Fig. 7, and that the average Cr content in M_3C particles in M3:2 increased approximately 5.5% to approximately 21.7% in the MN2 steel, leading to the higher stability of the M_3C even after such a long tempering time. Because little M_3C precipitated in MN2 steel after overtempering for 96 h at 600 °C and because the fine MC and M_2C dispersion was not markedly changed by this treatment, we conclude that the steel was still supersaturated with respect to the precipitates after this treatment. This conclusion is consistent with observations of continued precipitation when tempering for 168 h at 600 °C and with the measurements of high Cr and Mo content in the matrix, as shown in Table 2.

Note that the size of MC precipitates was relatively constant during tempering; by contrast, the size of M_2C increased during overaging. After 168 h of overaging, the size of the MC precipitates started to increase. In the present case, even though

the content of Nb in primary MC carbides in MN2 reached 52% due to its high affinity with carbon, however, the volume fraction of undissolved MC carbides in this steel prior to tempering has reached 2.97%, more than double those in the M3:2 (1.38%). As a result, the solid solubility of V that can be used for precipitation of MC carbides from the matrix of MN2 during tempering is less favorable compared to the M3:2 steel (Table 2). In this case, the effect of Nb addition on the distribution of MC precipitates was shown to be insignificant. Therefore, it can be confirmed that the effect of Nb on the as-tempered hardness is due to its effect on the distribution and stability of the M_2C precipitates within the tempered martensite, in addition to retarding the growth of M_3C carbides.

5. Conclusions

TEM was used to study the effect of Nb addition on the precipitation of carbides in spray-formed M3:2 HSS during tempering. The main results can be summarized as follows:

1. Repeated tempering at 560 °C results in the transformation of retained austenite to martensite and the very fine-scale precipitation of MC and M_2C secondary carbides, which is responsible for the secondary hardening peak at 560 °C.
2. During tempering under conditions of 3 × 1 h at 600 °C, the original M_2C secondary carbides in M3:2 coarsened but to a lesser degree in the Nb-containing steel.
3. Ellipsoidal M_3C gradually precipitates at the interfaces and within martensite plates during overaging at 600 °C. These reactions occur at the expense of the fine MC and M_2C secondary carbide dispersions.
4. Overaging for 168 h at 600 °C results in a partially recovered ferrite microstructure with coarse $M_{23}C_6$ and M_6C. Long rod-like-shaped M_3C measuring approximately 120-400 nm is found to precipitate on the boundaries of the internal twins and within the matrix in M3:2 steel, while very fine M_2C precipitates are also evenly distributed in MN2 steel.
5. It is suggested that the beneficial effect of Nb on the hot strength of M3:2 steel is due to a promotion of high-density and fine M_2C precipitates and a suppression of M_3C precipitate growth.
6. MC secondary precipitates are thermodynamically stable and show little tendency to coarsen; the number density increases during the first 96 h of overtempering at 600 °C, and there is no substantial difference in the population of MC precipitates between M3:2 and MN2 steels.

Acknowledgment

This research was financially supported by the State Key Development Program for Basic Research of China (Grant No. 2011CB606303), Open Foundation of State Key Laboratory for Advanced Metals and Materials, University of Science and Technology Beijing (Grant No. 2018-Z01), Program of the University Students' Innovation and Pioneering (Grant No. XZG-16-08-15) and Ph.D. Research Startup Project of Jiangxi University of Science and Technology (Grant No. 3401223322). The authors thank Dr. Zhang Jinxiang, Dr. Lu Lin, Mr. Xiyu He, Ms. Panpan Jiang and Ms. Lili Zhao for their help with materials preparation and academic discussions.

References

1. C.K. Kim, J.I. Park, S. Lee, Y.C. Kim, N.J. Kim, and J.S. Yang, Effects of Alloying Elements on Microstructure, Hardness, and Fracture Toughness of Centrifugally Cast High-Speed Steel Rolls, *Metall. Mater. Trans. A*, 2005, **36**, p 87
2. T.V. Pirtovšek, G. Kugler, M. Godec, and M. Terčelj, Three Important Points that Relate to Improving the Hot Workability of Ledeburitic Tool Steels, *Metall. Mater. Trans. A*, 2012, **43**, p 3797
3. W.H. Dennis, Refining Carbide Size Distributions in M1 High Speed Steel by Processing and Alloying, *Mater. Charact.*, 2001, **46**(2–3), p 175
4. P. Hellman, High Speed Steels by Powder Metallurgy, *Scand. J. Metall.*, 1998, **27**, p 44
5. K. Kumar, A. Lawley, and M. Koczak, Powder Metallurgy T15 Tool Steel: Part I. Characterization of Powder and Hot Isostatically Pressed Material, *Metall. Mater. Trans. A*, 1991, **22**, p 2733
6. Y.J. Lin, K.M. McHugh, Y.Z. Zhou, and E.J. Lavernia, Microstructure and Hardness of Spray-Formed Chromium-Containing Steel Tooling, *Scri. Mater.*, 2006, **55**, p 581
7. C. Cui, A. Schulz, and V. Uhlenwinkel, Co-spray Forming of Gradient Deposits from Two Sprays of Different Tool Steels Using Scanning Gas Atomizers, *Steel Res. Int.*, 2013, **84**, p 1075
8. M.M. Serna and J.L. Rossi, MC Complex Carbide in AISI, M2 High-Speed Steel, *Mater. Lett.*, 2009, **63**, p 691
9. R.A. Mesquita and C.A. Barbosa, Spray Forming High Speed Steel-Properties and Processing, *Mater. Sci. Eng. A*, 2004, **383**, p 87
10. K.M. McHugh, Y. Lin, Y. Zhou, and E.J. Lavernia, Influence of Cooling Rate on Phase Formation in Spray-Formed H13 Tool Steel, *Mater. Sci. Eng. A*, 2008, **477**, p 50
11. E. Lavernia and N. Grant, Spray Deposition of Metals: A Review, *J. Mater. Sci. Eng.*, 1988, **98**, p 381
12. P. Grant, Solidification in Spray Forming, *Metall. Mater. Trans. A*, 2007, **38**, p 1520
13. L.A. Dobrzanski, A. Zarychta, and M. Ligarski, High-Speed Steels with Addition of Niobium or Titanium, *J. Mater. Proc. Technol.*, 1997, **63**, p 531
14. R. Razavinejad, S. Firoozi, and S.M. Mirbagheri, Effect of Titanium Addition on as Cast Structure and Macrosegregation of High-Carbon High-Chromium Steel, *Steel Res. Int.*, 2012, **83**(9), p 861
15. Y.W. Yang, H.G. Fu, Y.P. Lei, K.M. Wang, L.L. Zhu, and L. Jiang, Phase Diagram Calculation and Analyze on Cast High-Boron High-Speed Steel, *J. Mater. Eng. Perform.*, 2016, **25**(2), p 409
16. F.S. Pan, P.D. Ding, S.Z. Zhou, M.K. Kang, and D.V. Edmonds, Effects of Silicon Additions on the Mechanical Properties and Microstructure of High Speed Steels, *Acta Metall.*, 1997, **45**(11), p 4703
17. S. Karagöz and H.F. Fischmeister, Niobium-Alloyed High Speed Steel by Powder Metallurgy, *Metall. Trans. A*, 1988, **191**, p 1395
18. J.H. Ahn, Y.J. Kim, S. Lee, and H. Chung, Effect of Niobium on the Mechanical Properties of Powder-Metallurgy Processed High-Speed Steels, *Z. Metallkd.*, 2005, **96**, p 1426
19. Y. Yu, J. Huang, H. Cui, Y. Cai, and J. Zhang, Effect of Nb on the Microstructure and Properties of Spray Formed M3 High Speed Steel, *Acta Metall. Sin.*, 2012, **48**, p 935
20. H. Halfa, M. Eissa, and K. EI-Fawakhry, Effect of Nitrogen and Niobium on the Structure and Secondary Hardening of Super Hard High Speed Tool Steel, *Steel. Res. Int.*, 2012, **83**(1), p 32
21. S.S. Gill, J. Singh, R. Singh, and H. Singh, Effect of Cryogenic Treatment on AISI, M2 High Speed Steel: Metallurgical and Mechanical, *J. Mater. Eng. Perform.*, 2012, **21**(7), p 1320
22. R. Wang, H. Andrén, H. Wisell, and G. Dunlop, The Role of Alloy Composition in the Precipitation Behavior of High Speed Steel, *Acta Metall. Mater.*, 1992, **40**(7), p 1727
23. H. Fishmeister, S. Karagöz, and H. Andrén, An Atom Probe Study of Secondary Hardening in High Speed Steels, *Acta Metall.*, 1988, **36**(4), p 817

24. A.S. Chaus and M. Domankova, Precipitation of Secondary Carbides in M2 High-Speed Steel Modified with Titanium Diboride, *J. Mater. Eng. Perform.*, 2013, **22**(5), p 1412
25. L. Lu, L. Hou, J. Zhang, H. Wang, H. Cui, J. Huang, Y. Zhang, and J. Zhang, Improved the Microstructures and Properties of M3:2 High-Speed Steel by Spray Forming and Niobium Alloying, *Mater. Charact.*, 2016, **117**, p 1
26. H.B. Wang, L.G. Hou, J.X. Zhang, L. Lu, H. Cui, and J.S. Zhang, The Secondary Precipitates of Niobium-Alloyed M3:2 High Speed Steel Prepared by Spray Deposition, *Mater. Charact.*, 2015, **106**, p 245
27. H. Leitner, P. Staron, H. Clemens, S. Marsoner, and P. Warbichler, Analysis of the Precipitation Behavior in a High-Speed Steel by Means of Small-Angle Neutron Scattering, *Mater. Sci. Eng. A*, 2005, **398**, p 323
28. V.G. Gavriljuk, V.A. Sirosh, Y.N. Petrov, A.I. Tyshchenko, W. Theisen, and A. Kortmann, Carbide Precipitation During Tempering of a Tool Steel Subjected to Deep Cryogenic Treatment, *Metall. Mater. Trans. A*, 2014, **45**, p 2453
29. A. Gingell, H. Bhadeshia, D. Jones, and K. Mawella, Carbide Precipitation in Some Secondary Hardened Steels, *J. Mater. Sci.*, 1997, **32**, p 4815
30. R.C. Thomson, Characterization of Carbides in Steels Using Atom Probe Field-Ion Microscopy, *Mater. Charact.*, 2000, **44**, p 219
31. K. Stiller, L.E. Svensson, P.R. Howell, R. Wang, H.O. Andren, and G.L. Dunlop, High Resolution Microanalytical Study of Precipitation in a Powder Metallurgical High Speed Steel, *Acta Metall.*, 1984, **32**, p 1457
32. R. Wang and G. Dunlop, The Crystallography of Secondary Carbide Precipitation in High Speed Steel, *Acta Metall.*, 1984, **32**, p 1591
33. M.G. Wells, An Electron Transmission Study of the Tempering of Martensite in an Fe-Ni-C Alloy, *Acta Metall.*, 1964, **12**, p 389
34. H. Wang, L. Hou, J. Zhang, L. Lu, H. Cui, J. Huang, and J. Zhang, Microstructures and High Temperature Properties of Spray Formed Niobium-Containing M3 High Speed Steel, *Mat. Werkst.*, 2014, **45**, p 689
35. R. Tunney and N. Ridley, Effect of Alloying Elements on Rate of Ostwald Ripening of Cementite in Steel, *Acta Metall.*, 1972, **20**, p 867
36. S. Karagöz, H.F. Fischmeister, H.O. Andrén, and C.G. Jun, Microstructural Changes During Overtempering of High-Speed Steels, *Metall. Trans. A*, 1992, **23**, p 1631
37. A. Davenport and R. Honeycombe, The Secondary Hardening of Tungsten Steels, *Met. Sci.*, 1975, **9**, p 201
38. S. Bjorklund, L. Donaghey, and M. Hillert, Tempering of High-Purity and Commercially Based Steels Containing 10 wt% Tungsten or 5 wt% Molybdenum, *Met. Sci.*, 1979, **13**, p 585
39. H.M. Lee, S.M. Allen, and M. Grujicic, Coarsening Resistance of M_2C Carbides in Secondary Hardening Steels: Part I. Theoretical Model for Multicomponent Coarsening Kinetics, *Metall. Trans. A*, 1991, **22**, p 2863
40. G.L. Dunlop and R.W. Honeycombe, Ageing Characteristics of VC, TiC and (V, Ti)C Dispersions in Ferrite, *Met. Sci.*, 1978, **12**, p 367